Responses of Defect-Rich Zr-Based Metal-Organic Frameworks towards NH_3 Adsorption

Tatchamapan Yoskamtorn[1,#], Pu Zhao[1,#], Xin-Ping Wu[2,*], Kirsty Purchase[1], Fabio Orlandi[3], Pascal Manuel[3], James Taylor[3], Yiyang Li[1], Sarah Day[4], Lin Ye[1], Chiu C. Tang[4], Yufei Zhao[5], S.C. Edman Tsang[1,*]

[1]Wolfson Catalysis Centre, Department of Chemistry, University of Oxford, Oxford OX1 3QR, U.K.

[2]Key Laboratory for Advanced Materials, Centre for Computational Chemistry and Research Institute of Industrial Catalysis, East China University of Science and Technology, 130 Meilong Road, Shanghai 200237, P.R. China

[3]ISIS Neutron and Muon Source, Rutherford Appleton Laboratory, Didcot OX11 0QX, U.K.

[4]Diamond Light Source Ltd., Harwell Science and Innovation Campus, Didcot OX11 0DE, U.K.

[5]State Key Laboratory of Chemical Resource Engineering, Beijing University of Chemical Technology, Beijing, 100029, P.R. China

ABSTRACT: Understanding structural responses of metal-organic frameworks (MOFs) to external stimuli such as the inclusion of guest molecules, temperature/pressure has gained increasing attention in many applications, for example, manipulation and manifesto smart materials for gas storage, energy storage, controlled drug delivery, tunable mechanical properties, and molecular sensing, to name but a few. Herein, neutron and synchrotron diffractions along with Rietveld refinement and density functional theory calculations have been used to elucidate the responsive adsorption behaviors of defect-rich Zr-based MOFs upon the progressive incorporation of ammonia (NH_3) and variable temperature. UiO-67 and UiO-bpydc containing biphenyl dicarboxylate and bipyridine dicarboxylate linkers, respectively, were selected and the results establish the paramount influence of the functional linkers on their NH_3 affinity, which leads to stimulus-tailoring properties such as gate-controlled porosity by dynamic linker flipping, disorder, and structural rigidity. Despite their structural similarities, we show for the first time the dramatic alteration of NH_3 adsorption profiles when the phenyl groups are replaced by the bipyridine in the organic linker. These molecular controls stem from controlling the degree of H-bonding networks/distortions between the bipyridine scaffold and the adsorbed NH_3 without significant change in pore volume and unit cell parameters. Temperature-dependent neutron diffraction also reveals the NH_3-induced rotational motions of the organic linkers. We also demonstrate that the degree of structural flexibility of the functional linkers can critically be affected by the type and quantity of the small guest molecules. This strikes the delicate control in material properties at the molecular level.

INTRODUCTION

The development of smart materials for stimuli-responsive recognition, wherein a complex form in a manner that is sensitive to, or can be governed by, externally applied triggers such as light, temperature, pressure, magnetic or electric field has recently been receiving a lot of attention. Molecular engineering, biometric and design approaches offer an assortment of new chemistry and material design tools toward improving precision in tailoring properties. For example, understanding and controlling molecular motions of synthetic materials towards stimulus for their order-disorder transformation, reorientational and rotational motion associated with phase transitions may allow switching back and forth between hard or soft state, a breakthrough that offers an innovative solution to a long-standing challenge with synthetic materials by giving them both strength and shape adaptability.[1-3]

Metal-organic frameworks (MOFs)[4] or porous coordination polymers (PCPs)[5] are highly topical classes of porous crystalline solids, constructed by metal ions/clusters coordinated to functional organic linkers that are suitably under exploration in this area. They possess large surface area, high porosity, functional diversity and structural flexibility, which tremendously excites their use in many applications.[6-8] The rational design of MOF materials for applications heavily relies on a thorough understanding of the host-guest interactions of the frameworks with exterior triggers. The nature of these interactions if controllable has been considered to primarily manipulate the MOF structural properties such as disorder, flexibility, compressibility as well as chemical reactivity.[3] Recently, different gas sorption phenomena in MOFs have been recognized for efficient gas separation application.[9-14] Sequential pore filling in non-uniform MOF pores has also been attributed for differential gas sorption phenomena.[9-10, 15] Flexible and dynamics motions of MOF linkers that undergo rotation or libration have been elucidated to play a dramatic role in guest-induced gate opening phenomena in many MOFs such as ZIF-8[16], DUT-98[17], and Cu-based PCPs[14].

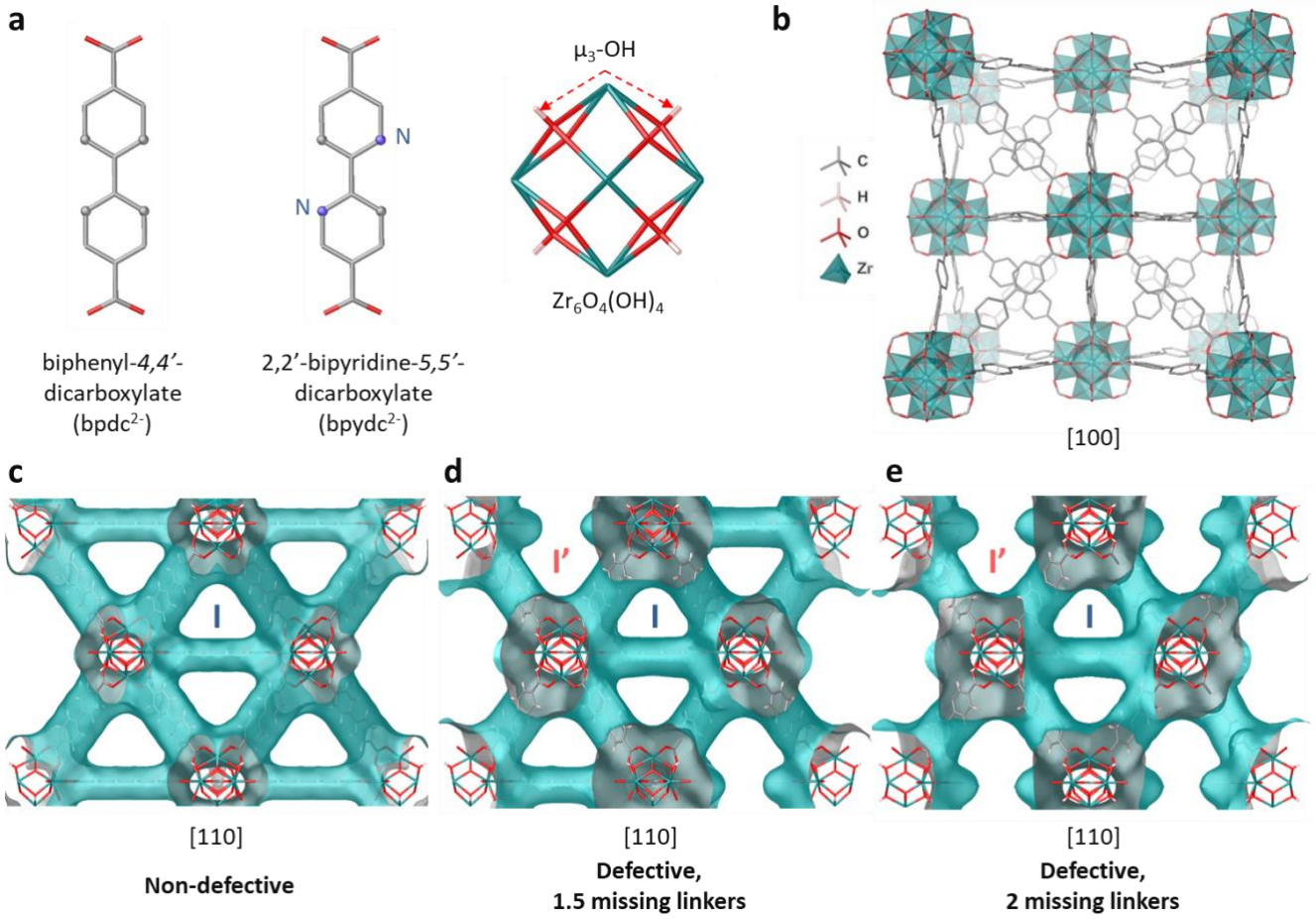

Figure 1 | Visualisation of the UiO-67 type MOFs. (**a**) Components including organic linkers and $Zr_6O_4(OH)_4$ nodes and (**b**) Crystal structure with a reticular formula of $Zr_6O_4(OH)_4(linker)_{6-x}(anionic\ capping\ species)_{2x}$, where x refers to the number of missing linkers per formula. (**c**) Solvent-excluded surface maps of non-defective and defective structures of the UiO-67 type MOFs with (**d**) 1.5 missing linkers per formula and (**e**) 2.0 missing linkers per formula. The radius of the probe sphere is 1.826 Å equivalent to the approximate Van der Waals radius of an NH_3 molecule. I and I' represent primitive triangular and lozenge windows caused by missing linker defects, respectively. The structures are illustrated by using polyhedral and stick models; Zr: teal, O: red, C: grey, N:

Blue, H: pale pink. H atoms in the linkers in (**b**) are omitted for clarity. I and I' represent trigonal and lozenge windows created by missing linkers, respectively.

Table 1 | Sample information used in the *in-situ* NPD experiments.

Sample	**UiO-67**				**UiO-bpydc**			
Reticular formula	$Zr_6O_4(OH)_4(bpdc)_{6-x}(acetate)_{2x}$				$Zr_6O_4(OH)_4(bpdc)_{6-x}(acetate)_{2x}$			
Actual reticular formula[a]	$Zr_6O_4(OH)_4(bpdc)_4(acetate)_4$				$Zr_6O_4(OH)_4(bpydc)_{4.5}(acetate)_3$			
Loading amount of ND_3 (mmol/g)	0.00	1.23	4.63	7.60	0.00	4.15	4.27	6.06
Loading amount of ND_3 (molecule/unit cell)	0.00	9.65	36.3	59.6	0.00	32.6	33.6	47.6
Loading temperature (K)	300				300			
Measurement temperature (K)	300 and 7			300 and 150	300 and 7			

[a] Based on the ICP-MS data in the Supplementary Information.

The previously introduced structural transitions of MOFs, however, experience large volume change both in the nanospace and in the bulk solids challenging the practical use of these materials, especially in sorption-based applications.[18] This volume expansion in the adsorbent solid is disadvantageous as it may damage the storage tank, decompose the moldings, and also may result in slower diffusion of gases in the tank. Consequently, design of new porous 'rigid' materials that can show guest adsorption and desorption with specific interaction(s) without significant volume change is highly desirable and technologically important. For example, Kitagawa and co-workers showed by SXRD and refinement of their crystalline MOFs and porous coordination polymer (PCP) that the polarised CH_2Br (also Cl and I) linker with CO_2 interaction can account for the additional CO_2 stepped uptake without significant structural or volume changes.[18] Similarly, Bärwinkel and co-workers demonstrate that additional capacity of adsorption for CO_2 was realized by their crystalline microporous organically pillared layered silicates (MOPS) from their SXRD and refinement using the interaction of CO_2 with the organic cationic pillar based on electrostatic interactions without any framework and macroscopic pore volume changes.[19]

In addition, studying the flexibility of MOF's organic linker by guest molecule stimulus at variable temperature may provide hints about their molecular interaction. To our understanding, flexible MOFs are characterized mainly by changes in the pore structure. For example, the "flexibility" is well-known to occur in phenylene-based ligand systems.[14, 20-21] Gonzalez-Nelson *et al*.[2] have recently reviewed the studies of rotational barriers and dynamics of such ligand motives upon guest inclusion from the literature. However, these works were set in context to materials that exhibit large changes in unit cell and pore volume upon guest inclusion and other stimuli. The framework flexibility in the context of mainly ligand "flipping" but without significant pore volume alteration remains almost unexplored.

Zr-based MOFs UiO-66 and UiO-67[22] are well known for their robust yet defect-rich structures.[23-24] The effect of defects on the CO_2 adsorption behavior of UiO-66 has been demonstrated previously.[25] Thus, the tailoring the framework to accommodate controllable missing linkers as demonstrated can have a strong impact on the materials' properties, both by changing the characteristics of the pore windows of the MOF and by controlling the access to internal sites in pore cavities. Further incorporation of hydrogen bond functionality directly into MOF for gas uptake and molecular recognition is also thought to be important for the fine-control.[3, 26] As a result, new properties such as flexible gate-opening behavior (transition between a closed and open form) with higher resistance to structural collapse can be anticipated for a wide range of future nanotechnology applications.[15-27]

Here, defective UiO-67 with its organic linkers is selected to demonstrate how its non-monodisperse pore structure created by missing linker defects affect its NH_3 adsorption behavior. Sequential pore filling induced by different pore openings created by ligand defects leads to a two-step NH_3 adsorption isotherm in UiO-67. While responsive behaviors of MOFs to weakly interacting molecules such as hydrogen, carbon dioxide, and hydrocarbon have been widely explored,[9-11, 27-29] only a few reports focused on more polar coordinating gases such as water, alcohols, and NH_3.[12, 17,30-31] In addition, although unusual adsorption behaviors for polar coordinating gases have been observed[12, 17, 30, 32], in-depth study on sorption mechanisms and structural responses of MOFs is rarely explored at the molecular level. In this study, *in situ* high-resolution neutron and synchrotron powder diffractions (NPD and SXRD) combined with density functional theory (DFT) calculations were used to study the precise binding domains and the structural interactions of NH_3 with UiO-67 framework. Although NPD has been used to study NH_3 adsorption in UiO-67[33], detailed investigation of host-guest interactions in this material has not been reported before. To further engineer defects in UiO-67 to create a polar surface porous structure for controlled NH_3 adsorption, we synthesized defective UiO-bpydc by replacing the phenyl

groups of biphenyl-*4,4′*-dicarboxylate (bpdc) linkers in UiO-67 with pyridine groups.[34-35] Thus a UiO-67 isostructure with different pore surface polarity is designed to fine-tune its NH_3 adsorption profile. Here, we show that H-bonding networks can be formed between the bipyridine scaffold and the adsorbed NH_3. They offer a steric hindrance to modify the NH_3 adsorption behavior, disorder, and structural flexibility of the framework without major structural or pore volume change, indicating the importance of host-guest interactions on controlling the responsive behaviors of the MOFs with the trapped molecules upon external triggers. This work provides a microscopic picture of porosity tailoring, disorder, and flexibility of MOFs with designated functional linkers by tunable NH_3 adsorption at different temperatures.

RESULS AND DISCUSSION

UiO-67[22] and UiO-bpydc[34-35] are isostructural MOFs consisted of Zr_6 oxoclusters coordinatively bound with biphenyl-*4,4′*-dicarboxylate (bpdc) and *2,2′*-bipyridine-*5,5′*-dicarboxylate (bpydc) linkers, respectively. Thanks to the high connectivity of Zr_6 oxoclusters, UiO-67 and UiO-bpydc can retain their crystal structures even with the occurrence of missing linkers. The degree of defects induced by missing linker can be manipulated during the synthesis procedure by using various capping molecules (e.g. acetate). The chemical formula of the UiO-67 and the UiO-bpydc are written as $Zr_6O_4(OH)_4(bpdc)_{6-x}$(anionic capping species)$_{2x}$ and $Zr_6O_4(OH)_4(bpydc)_{6-x}$(anionic capping species)$_{2x}$ where x refers to the number of the missing linkers per formula. UiO-67 and UiO-bpydc exhibit the same crystal structures with space group *Fm*-3*m*. Their crystal structures with fcu topology are depicted in Figure 1. Without defects, the structures consist of uniform trigonal windows with the diameter of 11 Å that lead to interconnected tetrahedral and octahedral pores inside the structures (Figure 1c). For the tetrahedral and octahedral pores, their pore size is defined as the diameter of the biggest sphere that can be fitted into the specific pore (12 and 16 Å). In the presence of missing linker defects, the trigonal windows surrounding the defects are merged into lozenge windows with a dynamic size larger than 14 Å (Figure 1d and 1e). For clarity, UiO-67 and UiO-bpydc with defects will be referred to as "UiO-67" and "UiO-bpydc" throughout the paper, respectively, unless otherwise specified.

XRD, elemental analyses, TG, and N_2 sorption analyses were employed to verify structural properties and compositions of the prepared MOF samples (Figures S2-S9). These values suggest a significant degree of missing linker (defects), which generally agree well with the previous report that used monocarboxylic acid as the modulator.[22] The analysis results of the defective MOFs after healing process[36] also reveal the repairing some of the linker density for the UiO-67 and the UiO-bpydc samples. The post-healing process gives narrower pore size distributions which can be clearly observed (Figures S8 and S9). There is a sharp increase of the pores centred at around 11 Å along with a general reduction of larger pores after the defect healing process. These observations confirm that the missing linker defects indeed pervasively exist and potentially affect the pore structure. After the healing process, we did not observe any significant change in the pore volume as similar to that of the previous works.[18,19] Although it is known that defects could affect pore volume, the observed change in the pore size distribution is more likely to reflect the change in the quantities of the windows rather than the interior pores.

NH_3 adsorption in defective UiO-67

Information on the sample properties involved in the NH_3 adsorption analyses and the NPD experiments are summarized in Table 1. NH_3 sorption isotherms measured at 298 K and up to 1100 mbar of NH_3 pressure are shown in Figure 2 (bottom left). First, the profile of adsorption clearly displays a 'step-like shape' with two clear transitions. Such behavior in MOFs is mainly caused by a gate-opening phenomenon: the interaction between guest molecules and pore walls, or a pore filling process, in particular for a polar fluid such as water and NH_3 with nonpolar walls, whereas the change in framework size plays a minor role. [18,19] At the beginning of adsorption, there is a rapid and abrupt increase of over 1.70 mmol/g NH_3 uptake at an NH_3 pressure lower than 30 mbar (Position I). This result indicates the presence of strong adsorption sites inside the framework, likely due to the readily binding of NH_3 with either μ_3-OH in Zr_6 oxoclusters or missing linker defects. According to defect stoichiometry, the concentration of μ_3-OH of UiO-67 is estimated to be 1.91 mmol/g, which is comparable to the amount of NH_3 adsorbed. Therefore, we assign the majority of the initial adsorption to the NH_3 interaction with μ_3-OH. The uptake suddenly increased from 2.40 to 4.40 mmol/g at an NH_3 pressure of 250 mbar (Position II) and 5.60 to 8.40 mmol/g at an NH_3 pressure of 650 mbar (Position III) as the two transition points. These results suggest two strong but discrete changes in the interaction(s) of the MOF-NH_3 system upon increasing NH_3 partial pressure. In the desorption isotherms, large opened hysteresis loops were found, implying that the strongly bound NH_3 molecules resistively remain inside the framework, defying the adsorption-desorption reversibility. However, these bound NH_3 molecules can be fully desorbed by treating the samples at 423 K for 1 h under dynamic vacuum (Figure S10). NH_3 stability of UiO-67 was investigated by testing NH_3 sorption for three cycles and exposing the materials to NH_3 vapor for one week. In contrast with previous work,[33] no significant change of structures was found in XRD patterns of NH_3-loaded MOFs (Figure S11) and no shift of IR spectra in carbonyl region indicating the same binding mode of carboxylate linkers upon NH_3 incorporation (Figure S12). These results confirm the high stability of the materials for the NH_3 uptake experiments. To understand the origin of the interesting stepwise MOF-NH_3 interactions at the molecular level, *in situ* high-resolution neutron powder diffraction (NPD) experiments supported by synchrotron X-ray powder diffraction (SXPD) were carried out at WISH beamline, ISIS Neutron, and Muon Source, and Diamond of the UK STFC facilities, respectively. This analysis, particularly the NPD, is a powerful tool to study MOF materials that contains both heavy and light elements. Unlike X-ray diffraction, neutron diffraction is sensitive to both organic linkers and metal

clusters because the coherent neutron scattering cross-sections (σ_c) are independent of Z^2, where Z is an atomic number. The σ_c values of Zr, O, C, N, and D are 6.44, 4.23, 5.55, 11.01, and 5.59 barns, respectively.[37] Fully deuterated ammonia (ND_3) was used in these NPD experiments to minimize the incoherent scattering from H. This allows for a high diffraction contrast between the ND_3-loaded and the guest-free materials. The use of SXPD allowed complementary analysis (see in the supplementary information, SI)

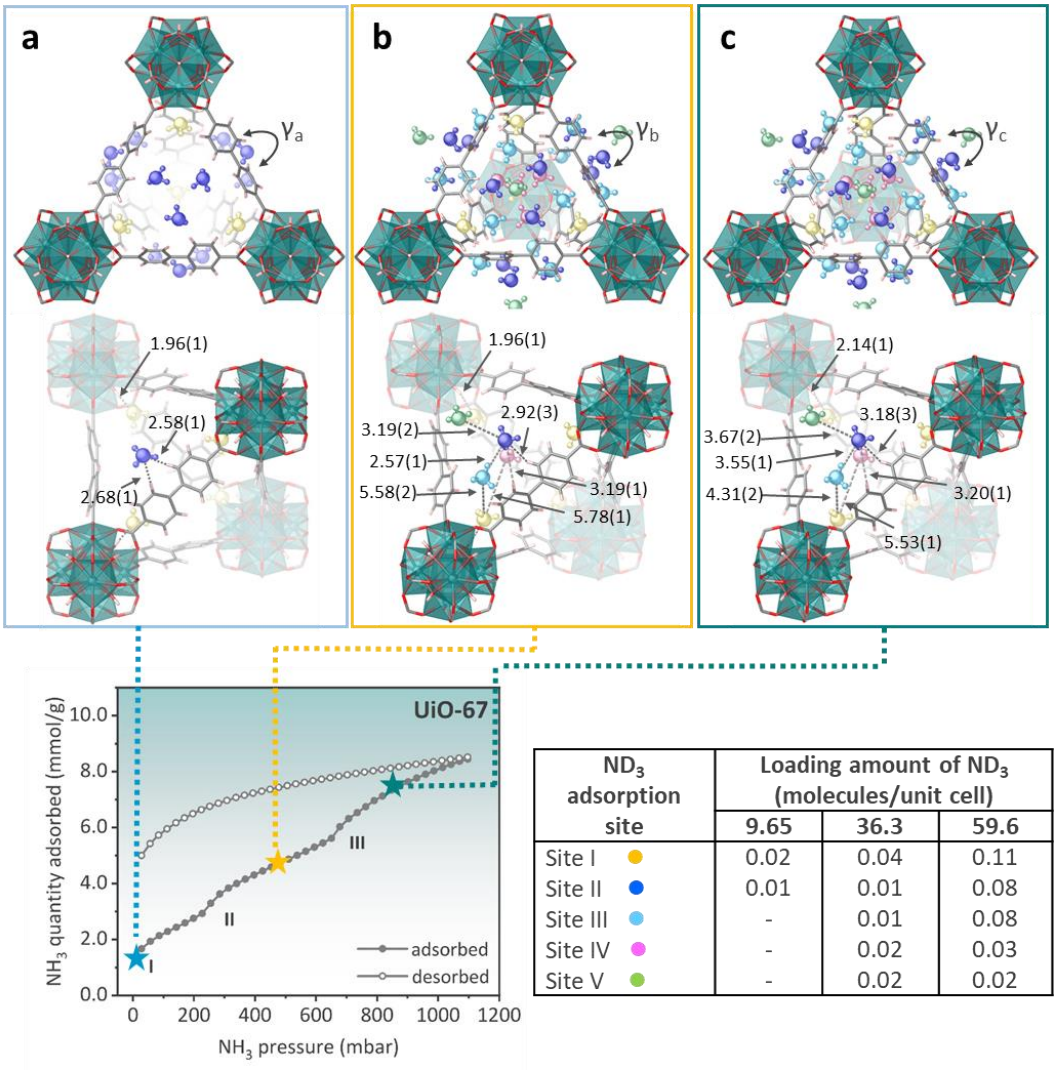

ND_3 adsorption site	Loading amount of ND_3 (molecules/unit cell)		
	9.65	36.3	59.6
Site I	0.02	0.04	0.11
Site II	0.01	0.01	0.08
Site III	-	0.01	0.08
Site IV	-	0.02	0.03
Site V	-	0.02	0.02

Figure 2 | ND_3 responsive behaviors of the defective UiO-67. Refined ND_3 positions in the UiO-67 structure at the ND_3 loading of **a**) 1.23, **b**) 4.63, and **c**) 7.60 mmol/g obtained from NPD data at 300 K which are equivalent to 9.65, 36.3, and 59.6 ND_3 molecules per unit cell. Each of the structures is refined and shown in top and side views of the trigonal window. Ball and stick models with different colors represent ND_3 molecules at different binding sites; site I: yellow, site II: blue, site III: light blue, site IV: pink, and site V: green. The host structures are illustrated by using polyhedral and stick models; Zr: teal, O: red, C: grey, H: pale pink. Only tetragonal pores are depicted and the symmetry of ND_3 is disregarded for clarity. The dihedral angles between two phenyl rings (γ) are 32.19(1)°, 55.20(1) °, and 63.62(2) ° for γ_a, γ_b, and γ_c, respectively. The number in round brackets are referred to as an estimated standard deviation. The associated NH_3 sorption isotherm at the bottom left was measured at 298 K and up to 1100 mbar of NH_3 pressure; adsorption: closed circles; desorption: open circles).

The NPD data of UiO-67 at different dosing amount of ND_3 were measured at 300 K to correlate the refined adsorption structures to the observed adsorption profiles at 298 K. The corresponding structural information, including atomic coordinates, orientations, and occupancies, were thoroughly analyzed by using Rietveld refinement method[38] in TOPAS-Academic 5 software[39]. Details of data analysis are available in the SI.

A series of NPD patterns for the adsorption of ND_3 by UiO-67 is shown in Figure S13. Some new Bragg peaks were clearly observed with a significant increase of peak intensity at the increasing quantity of ND_3 dosing. In contrast, the relative intensities of original peaks became reduced and their peak ratios significantly altered. These results can be caused by a structural modification of the MOF structure induced by both the orderly binding of the ND_3 molecules[33] and the dynamic motions of the MOF

linkers. One might attribute the pronounced changes in diffraction patterns to the subtle deformation of the framework. However, Rietveld refinement confirms that there is no apparent change of the unit cell parameters upon the ND_3 inclusion over the range of NH_3 pressure used in this study (Figure S15). This observation suggests that peak intensities and positions can also be altered by guest loading without any change in structure.

Crystal structure refinement based on the high-resolution NPD data can directly reveal the existence of missing linker defects.[25] If the missing linker defects occur randomly in the MOF structure, the linker occupancies in the lattice points should be lower than unity in the refinement. We, therefore, investigated this hypothesis by refining the structures of guest-free UiO-67 using the hydroxylated structure models reported in the literature.[34, 40] All atoms of the organic linkers were freely refined. The initial refinements revealed that the linker occupancies of the UiO-67 sample were clearly much less than 100 %. The much-improved values of fitting for bare UiO-67 with negligible residual nuclear density were achieved when we freely refined the occupancies of the central part of its corresponding linker ($[C_{12}H_8C_2]$), but left Zr fully coordinated by carboxylate O. The obtained occupancy of the UiO-67 linker was determined to be 48.38 % with R_{wp}/ R_p/ R_{exp}/ GOF values of 1.77 %/ 1.32 %/ 0.47 %/ 3.78 (Table S3 and S4). These values are in an agreement with the elemental analysis within experimental error, which confirms the presence of missing linker defects in these samples (Table S1 and S2).

During the refinement, as previously stated, there is consistently lower occupancy of organic linker than carboxylate O atoms which implies that some O-type terminal groups still bind to unoccupied Zr nodes in the missing linker defects even after activation at 423 K for 24 hours under dynamic vacuum. We ruled out water (H_2O) as the defect-capping group since there were no significant nuclear residues at a position that was reported to be a site of the bound water molecule.[41] This sounds sensible because the activation condition should be sufficient to completely remove the trapped water from the samples. We then considered hydroxyl (–OH) and acetate ($-OOCCH_3$), as possible candidates. The latter was more likely to us since the best fitting values were gained when the Zr nodes were fully coordinated by carboxylate O atoms as mentioned above. Site occupancies of the carboxylate C and the Ipso C of the aromatic rings are also 11.79% higher than those of the remaining linker atoms, suggesting that additional carboxylate molecules could possibly locate at the defect sites, yet in a disorderly binding configuration. The occurrence of acetates as the terminating groups is further confirmed by the ^1H NMR spectrum of the digested UiO-67 and UiO-bpydc samples (Figures S4, S5). We thus used these refined structures as initial models for refinement of the ND_3-loaded samples.

For the Rietveld refinement of the ND_3-loaded UiO-67, as previously stated, small but unindexed extra peaks was clearly found in the NPD patterns of the samples with 4.63 and 7.60 mmol/g ND_3 loadings (Figure S13b). This observation can be ascribed to the distortion of the cubic Fm-*3*m MOF structure by the inhomogeneous ND_3 uptake[42] (only a small quantity). Thus, in addition to using the single perfect MOF model (i.e. the model based on published crystal data and the occupancy number of linker with the assumption that the missing linker occurs randomly, the second MOF model with lowering the symmetry to cubic primitive cell (*Pa*-3 space group) to represent a small-distorted phase was applied to achieve the best fit of the refinement. The weight percentage of each phase was freely refined to give the final phase composition of 78.16% (*Fm*-3*m*) and 21.84% (*Pa*-3) with all the diffraction peaks well fitted (Figures S19 and S20 and Table S4). The refined crystal structures of the ND_3-loaded samples are available to download with free of charge from The Cambridge Crystallographic Data Centre (see SI for details of these crystal structures).

Figure 2a-c demonstrates the refined structures of UiO-67 at different ND_3 dosing derived from the NPD data at 300 K. All ND_3-loaded samples retain the *Fm*-3*m* space group but have crystallographic independent NH_3 binding sites resolved in each case. For ND_3-loaded UiO-67 with the lowest uptake before any pore filling (Figure 2a), there are two sites for ND_3 binding to the frameworks; site I (occupancy 0.02) and site II (occupancy 0.01). At site I, ND_3 molecule primarily adsorbs close to the μ_3-OH with a $OH\cdots N_I$ distance of 1.96(1) Å ($O\cdots N_I$ = 2.80(1) Å), as we previously discussed. This result indicates the formation of H-bonding interaction between the μ_3-OH and ND_3, comparable to the recent report from Godfrey *et al*.[43] Interestingly, ND_3 molecules at site II located near the walls of the trigonal windows indicative of some degree of interactions with the MOF organic linkers ($H_{linker}\cdots N_{II}$= 2.58(1) and 2.68 (1) Å). Notice that the nonpolar phenyl rings of the biphenyl-*4,4′*-dicarboxylate (bpdc) linker may have formed a very weak dipole-induced dipole with each ND_3 molecule under this low adsorption quantity. Upon increasing the ND_3 dosing to 4.63 mmol/g or 36.3 ND_3 molecules/unit cell (Figure 2b), the site I occupancy clearly increase, indicating that more ND_3 molecules are adsorbed near the μ_3-OH. Apparently, further ND_3 molecules can be undoubtedly identified near the tetragonal pore by the structural refinement (site III and site IV). At site III, the ND_3 molecule filled the shallow pore positions with $N_{II}\cdots N_{III}$ bond distances among these ND_3 sites are in the range of 2.33(1) and 2.57(1) Å, indicating a H-bond network of these ND_3 molecules[44] spreading towards the filling of tetragonal pores from the ND_3 site II, presumably through the trigonal windows. Similarly, the inner pore site IV and a deep octahedral pore site V are also found occupied with ND_3, presumably through the growth of the H-bonding network. The progressive step-wise filling of the tetragonal pore is clearly shown due to the larger internal volume of the pore compared to the surface linker sites in the first transition step. When further dosing ND_3 beyond the second transition step (Figure 2c), higher occupancies of all the readily adsorbed sites are clearly observed. According to the refined structure, site V with interior filling of octahedral pores were observed along with an increase in its occupancy. Again, the $N_V\cdots N_{II}$ bond distances of ND_3 at site V from site II are in the range of 3.67(2) and 4.20(2) Å, indicating the growth of H-bonding

network in filling the octahedral pores presumably through the lozenge windows. The larger second transition step than the first one in the adsorption isotherm is in line with the expectation of the larger volume of octahedral pore and the higher partial pressure is required to fill the larger pore window.

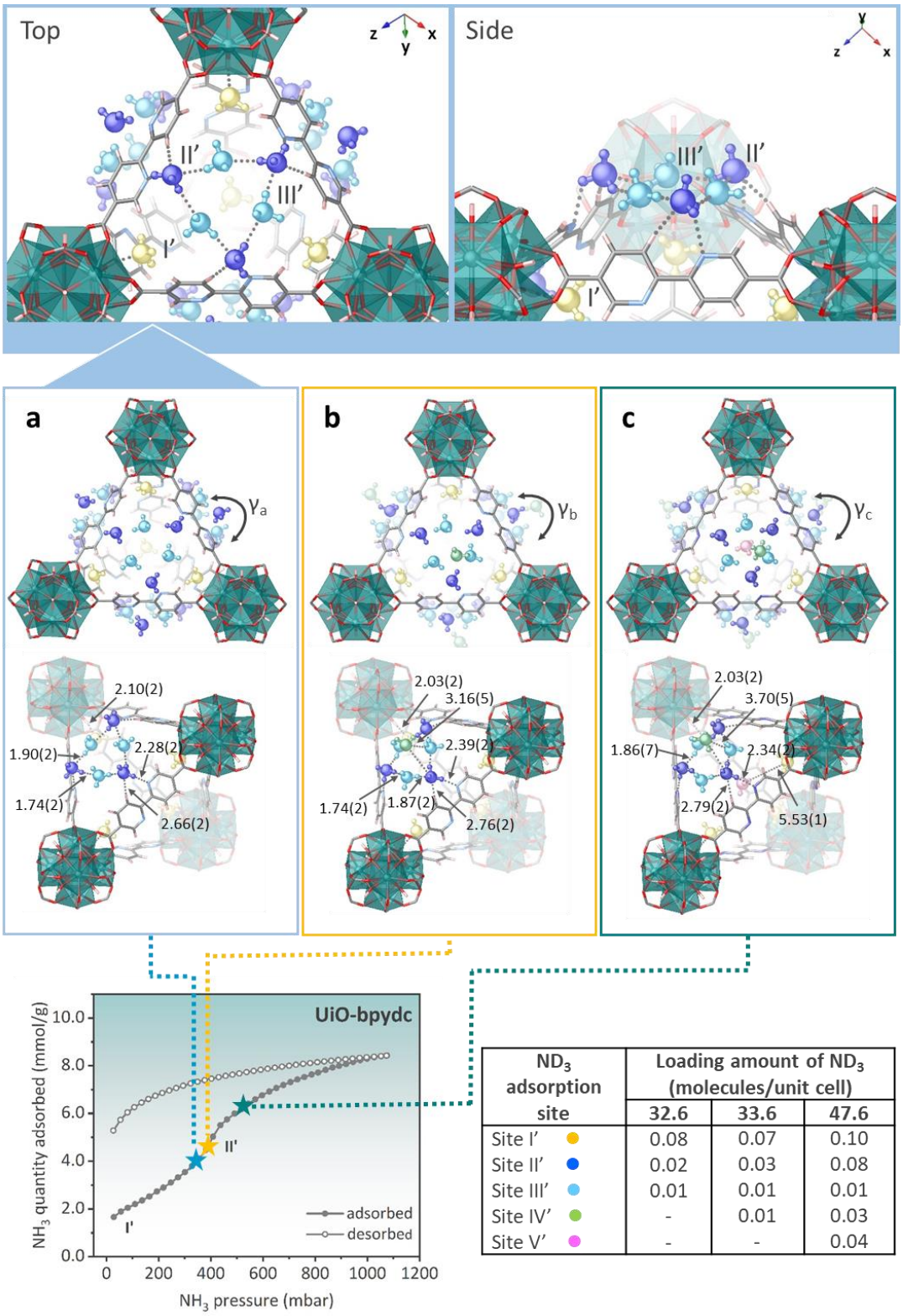

ND_3 adsorption site	Loading amount of ND_3 (molecules/unit cell)		
	32.6	33.6	47.6
Site I′	0.08	0.07	0.10
Site II′	0.02	0.03	0.08
Site III′	0.01	0.01	0.01
Site IV′	-	0.01	0.03
Site V′	-	-	0.04

Figure 3 | ND_3 responsive behaviors of the defective UiO-bpydc. Refined ND_3 positions of the UiO-bpydc structure at ND_3 dosing of **a**) 4.15, **b**) 4.27, and **c**) 6.06 mmol/g obtained from NPD data at 300 K which are equivalent to 32.6, 33.6, and 47.6 ND_3 molecules per unit cell. Each of the structures is shown in top and side views of the window. Ball and stick models with different colors represent ND_3 molecules at different binding sites; site I′: yellow, site II′: blue, site III′: light blue, site IV′: green, site V′: pink. The host structures

are illustrated by using polyhedral and stick models; Zr: teal, O: red, C: grey, N: blue, H: pale pink. Only tetragonal pores are depicted and the symmetry of ND_3 is disregarded for clarity. Units of bond distances are in angstrom (Å). The dihedral angles between two pyridine rings (γ) are 19.95(1) °, 16.77(3) °, and 10.00(4) ° for γ_a, γ_b, and γ_c, respectively. The number in round brackets are referred to as an estimated standard deviation. The associated NH3 sorption isotherm at the bottom left was measured at 289 K and up to 1100 mbar of NH_3 pressure; adsorption: closed circles; desorption: open circles).

In parallel with the trigonal windows in defect-free structure, the larger lozenge windows in our synthesized sample with the second transition (position III in Figure 2, bottom left) are thought to be generated by the missing linker defects, resulting in two distinctive stepwise adsorptions (Figure 2). The differences in pore shapes (tetragonal and octahedral) are not considered in the explanation of stepped NH_3 adsorption. This is because multilayer adsorption is not reflected in the adsorption isotherm of microporous materials and monolayer adsorption is hardly effected by pore shapes.[45] Comparison of NH_3 adsorption isotherms of unhealed (defective) and healed UiO-67 samples also supports this explanation (Figure S21). The adsorption step of the healed UiO-67 at higher NH_3 relative pressure was found almost disappeared. This undoubtedly reflects the relationship of the lozenge windows with the second transition step of NH_3 adsorption. The relative site occupancies of the material under exposure to ND_3 at different loadings with sufficient equilibration time may be more related to their adsorption affinity of the linker to the adsorbate rather than the molecular pathway for filling, which have not yet been studied in detail.[18,19]

NH_3-induced linker flipping in defective UiO-bpydc

To further engineer defective UiO-67 for controlled NH_3 adsorption, we synthesized defective UiO-bpydc by replacing the phenyl groups of biphenyl-*4,4'*-dicarboxylate (bpdc) linkers in UiO-67 with bi-pyridine groups.[34-35] It is anticipated that UiO-bpydc will have stronger H-bonding interactions with NH_3. NH_3-TPD data (Figure S22) can demonstrate the above point. Three different desorption temperatures at approximately 140, 200, and 230 °C were observed for UiO-67 and these desorption temperatures are assigned to that of reversed filling from weaker binding to stronger binding (higher site number to lower site number). Notice that the desorption peaks of UiO-bpydc are shifted to higher temperatures, indicating that UiO-bpydc has stronger interactions with NH_3 molecules.

According to the NH_3 adsorption isotherm in Figure 3 (bottom left), UiO-bpydc exhibits NH_3 uptake as high as 8.4 mmol/g at 298 K and 1100 mbar of pure NH_3 gas, which is comparable to that of UiO-67 with similar unit cell parameters and pore sizes. However, unlike UiO-67, UiO-bpydc only has one large and sharper transition step (position II') in its NH_3 adsorption isotherm. The transition pressure P of 400 mbar is in between of those two (250 and 650 mbar) in the NH_3 adsorption isotherm of UiO-67. To further understand the origin of the interactions between NH_3 and UiO-bpydc, *in situ* NPD experiments were also carried out. NH_3 gas was replaced by ND_3 to get a better scattering signal. Diffraction patterns of the bare and ND_3-adsorbed UiO-bpydc are shown in Figure S23. Upon ND_3 dosing, peak intensities that correspond to the framework structure became weaker while small extra peaks with increasing intensities were observed (Figure S23b). The positions of the extra peaks differ from ones observed in UiO-67 samples. This implies different binding domains of the ND_3 molecules inside the structure of ND_3-filled UiO-bpydc. The existence of missing linker defects was also confirmed by Rietveld refinements of the NPD results (Table S12-S14), giving the quantification of defects comparable to the elemental analyses and TG data (Table S1 and S2).

Figure 3a-c demonstrates the refined structures of UiO-bpydc at different ND_3 dosings. First, we have considered the two points just below the transition step in the NH_3 adsorption. The UiO-bpydc displays much higher ND_3 loadings of 4.15 mmol/g (32.6 ND_3 molecules/unit cell, Figure 3a) and 4.27 mmol/g (33.6 ND_3 molecules/unit cell, Figure 3b) as compared to ~2.5 mmol/g of pre-step adsorption value in the case of the UiO-67. In the first pre-step point, we again observed two independent binding sites of ND_3 lying close to the μ_3-OH moiety (site I') and the organic linkers (site II', but this time, the bipyridine linker), respectively, before the extensive filling of the pores. This indicates that the adsorption of ND_3 readily takes place, particularly at site II', giving higher occupancy numbers. For site I', the $OH\cdots N_I$ bond distance is 2.10(2) Å, which is comparable to that found in the isostructural UiO-67 samples. This similarity of the $OH\cdots N_I$ distance in both UiO-67 and UiO-bpydc are indicative of identical primary strongest binding sites which result in the initial adsorption at the lowest partial pressure of ND_3 gas (position I' in Figure 3, bottom left). However, the three ND_3 at site II' of UiO-bpydc resides closer to each of the three organic linkers in the trigonal window with $N_{linker}\cdots D_{II'}$ and $H_{linker}\cdots N_{II'}$ lengths of 2.28(2) and 2.66(2) Å, respectively. This observation shown in Figure 3a reveals that the ND_3-bipyridine linker interaction is even stronger than the ND_3-biphenyl linker interaction with longer distances ($H_{linker}\cdots N_{II}$= 2.68(1), 3.19(1) and 3.20(1)) Å, Figure 2a, 2b, and 2c, respectively). Surprisingly, an extra binding of ND_3 at site III' was also observed in the shallow tetragonal pore, presumably forming the H-bonding network with the adsorbed three ND_3 molecules on each of the pyridine linkers of the trigonal window to give six bound ND_3 in total in this region. Thus, in UiO-bpydc, the measured $N_{II'}\cdots D_{III'}$ and $N_{III'}\cdots D_{II'}$ H-bonding distances between site II' and site III' initially built from adsorbed ND_3 on the N-containing linker around the trigonal window are 1.74(2) and 1.90(2) Å, respectively. This ND_3 configuration clearly depicts a H-bonding network of six ND_3 molecules with the three bipyridine linkers around the trigonal window. Further dosing of ND_3 molecules to the frameworks in the second pre-step point results in a surface closer site IV' above a H-bond packing of site II' and III' with a very low occupancy (0.01) (Figure 3b). Interestingly, almost no filling of any sites locating inside the tetragonal pore in this bipyridine linker which is significantly different from that of site III

(0.02) and site IV (0.01) of UiO-67 at comparable ND_3 pressure. The H-bonding network of ND_3 appears to have blocked up further ND_3 molecules to gain access to the interior pores through the trigonal window as that of the UiO-67 (Figure 3).

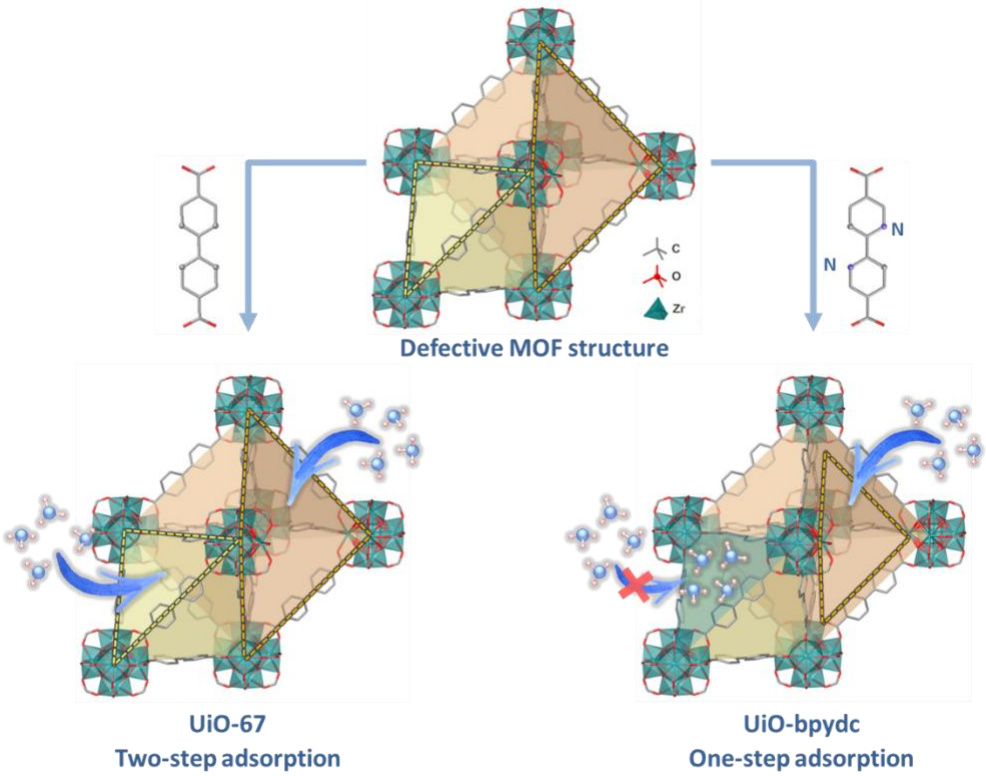

Figure 4 | Proposed NH_3 responsive behaviors of the defective UiO-67 type MOFs. The structures of the MOFs are illustrated by using polyhedral and ball& stick models; Zr: teal, O: red, C: grey, N: Blue, H: pale pink. H atoms in the linkers are omitted for clarity. Yellow and orange areas refer to tetragonal and octahedral pores, respectively, whereas yellow and orange dashed lines represent trigonal and lozenge windows, respectively.

It is interesting to see the drastic increase in the ND_3 loading to 6.06 mmol/g or 47.6 ND_3 molecules/unit cell at the post-step point (Figure 3c), approaching to the status that all pores are filled up by the ND_3 molecules (site occupancies are high). Before saturation, we also anticipate that a similar H-bonding network between ND_3 molecules with remaining organic linkers in defective MOF structure can be built up to modify the lozenge windows under intermediate ND_3 pressures. Dissimilar to the closing up of the trigonal windows by the imperative H-bonding network with the six ND_3 molecules, the larger lozenge windows created by missing and perhaps less ordered linkers may likely be modified to become new but smaller windows with the average size between the trigonal and lozenge windows (Figure 4). This can account for the merging of the two transition steps in UiO-67 to one in UiO-bpydc at the NH_3 pressure intermediate to those two step-pressures observed in the NH_3 adsorption isotherm of UiO-bpydc. This hypothesis is supported by realization of the correlation between the degree of missing linker defects and ND_3 adsorption behaviors using the defect-healed samples (Figure S21). For the healed UiO-67 sample, the total uptake did not change but the second transition step almost disappeared. In UiO-67, the second transition step is believed to strongly relate to the larger lozenge windows created by missing linker defects. According to the crystal structure of UiO-bpydc obtained at a ND_3 loading of 47.6 ND_3 molecules/unit cell (Figure 3c), a ND_3 molecule can be readily located inside the octahedral pore (site IV') presumably through the ND_3 modified lozenge windows since the trigonal windows are blocked up. Because the adsorption transition pressure is lower than the second transition pressure in UiO-67 attributed to adsorption through non-modified lozenge windows, lozenge windows in UiO-bpydc at high ND_3 loadings should have smaller diameters than the non-modified ones in UiO-67. This indeed indicates that the lozenge window is partially blocked by adsorbed ND_3. Thus, we show the gate-opening/closing behavior via linker flipping of UiO-bpydc upon ND_3 adsorption for potential applications that heavily involve the dynamics of the linkers and kinetically-controlled processes such as gas separation, molecular sieving, and molecular sensing (Figure 4).

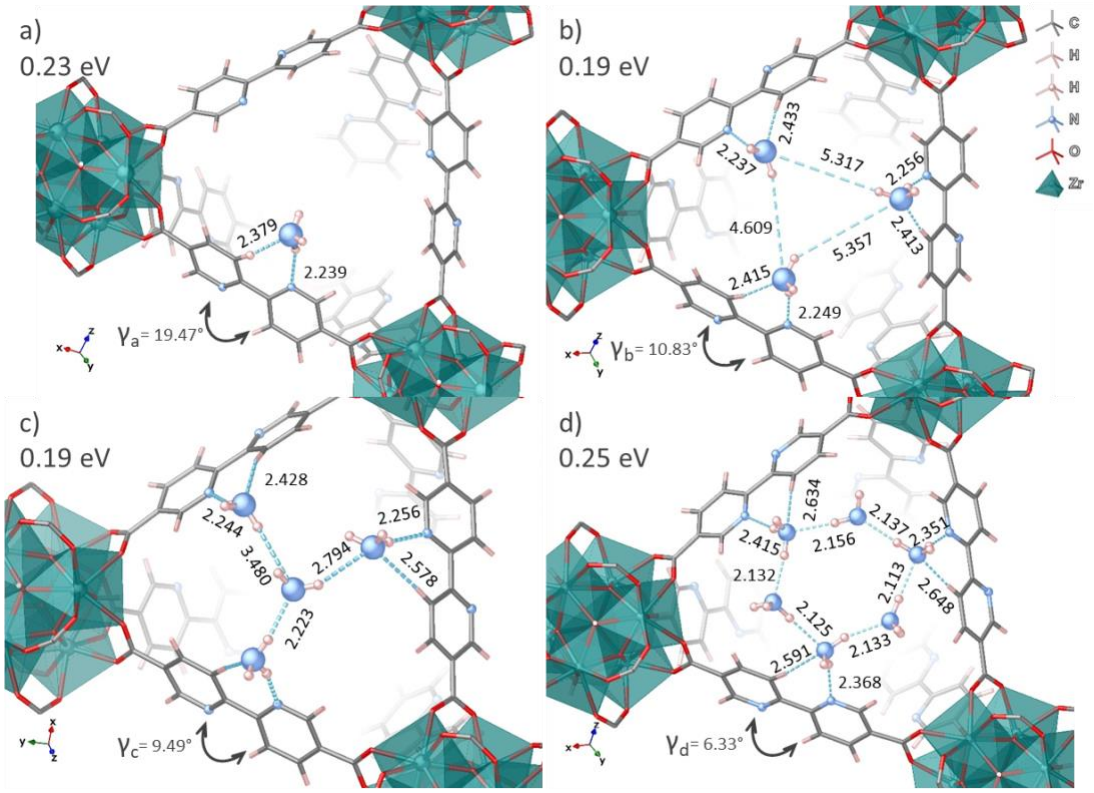

Figure 5 | Comparison of the MOF-NH_3 interactions by DFT calculations. DFT optimised structures of non-defective UiO-bpydc with *n* NH_3 molecules at the trigonal window: **a**) *n*=1; **b**) *n*= 3; **c**) *n*= 4; and **d**) *n*= 6. The corresponding binding energies are depicted at the top left of each image. The units of the H bond lengths and the specific atom–atom distances are in angstrom (Å). The dihedral angles between two aromatic rings are denoted as *γ*.

Analyses of the interactions by DFT calculations

DFT calculations were performed to investigate the role of the bipyridine linkers of UiO-bpydc in forming the H-bonding network with NH_3 molecules, in comparison with the biphenyl ones of UiO-67. The structures of UiO-67 and UiO-bpydc from Rietveld refinements with slight modifications were used as initial models for geometry optimisation. Since we focused on whether the extensive imperative H-bonding network could form at the trigonal windows of the two MOFs, we used the non-defective MOF structures for DFT calculations. The optimised configurations of the NH_3 molecules at the trigonal windows of UiO-67 and the corresponding binding energies are shown in Figure S31. The optimised desolvated structure of UiO-67 without NH_3 shows that the two phenyl rings with a freely rotated single C–C bond in the linkers prefer to align with each other with a dihedral angle (γ) of 31.27 °: this matches well with the literature value.[40] The calculated binding energy of 0.05 eV indicates the very weak interaction with ammonia molecule, which may be overcome at elevated temperature, giving no specific site binding (Figure S31a). Nevertheless, even in the absence of H bonding with the biphenyl linker of UiO-67, the NH_3 molecule at 0 K is still located near to the non-N containing linker due to dipole-induced dipole interaction. The binding energy is slightly enhanced to 0.06 eV per NH_3 molecule (Figure S31b) by further adding two more NH_3 molecules to the two remaining linkers of the trigonal window as similar to the refined structure in Figure 2a, depicting the consistent weak interactions. No further gain in binding energy (per NH_3 molecule) if NH_3 molecules were further added up to six.

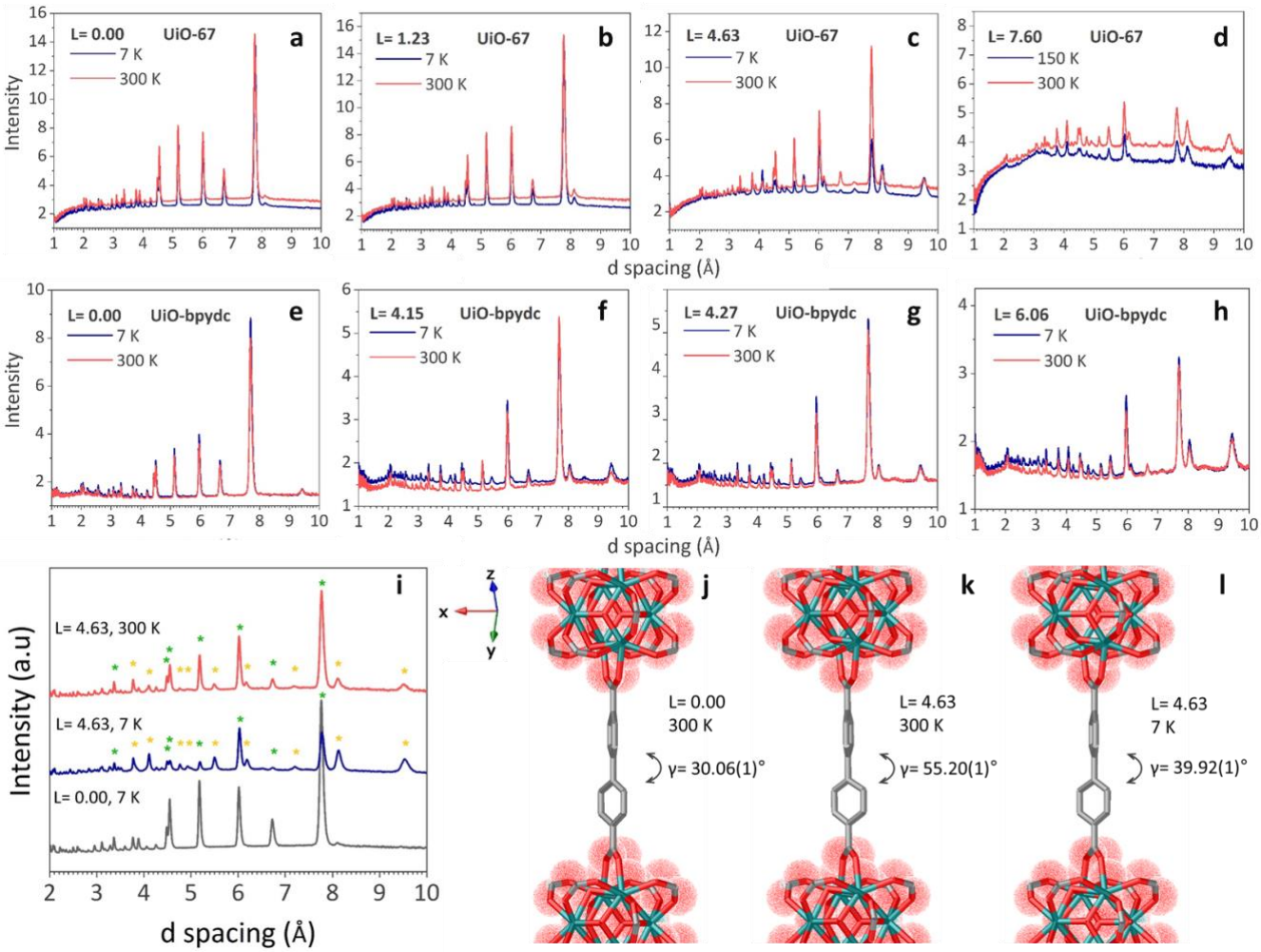

Figure 6 | Linker flexibility towards external stimuli. *In situ* NPD patterns of UiO-67 (**a-d**) and UiO-bpydc (**e-h**) at various loadings of ND_3 measured below 150 K and 300 K. Comparison of the NPD patterns of UiO-67 samples measured at different temperatures at L = 4.63 (36.3 ND_3 molecules/unit cell, **i**) and the refined structures at L= 0.00 mmol/g (**j**) and L= 4.63 (**k** and **l**), respectively. The data were collected on the 58.3 ° detector bank of the WISH diffractometer. L and γ refer to the dosing amount of ND_3 in mmol/g and the dihedral angles between biphenyl rings, respectively. Yellow asterisks indicate extra peaks (orderly packing of ND_3) after ND_3 dosing whereas green asterisks represent original peaks of the gas-free UiO-67. The host structures are illustrated by using a stick model; Zr: teal, O: red, and C: grey. H atoms and loaded ND_3 molecules are omitted for clarity.

Figure 5 demonstrates the optimised configurations and the binding energies of the NH_3 molecules at the trigonal windows of UiO-bpydc. It is clear to note that the binding energy for one NH_3 adsorption at the linker of UiO-bpydc (0.23 eV, Figure 5a) is much stronger than that of UiO-67 (0.05 eV, Figure S31a). In the case of UiO-bpydc, the binding energy is slightly attenuated to 0.19 eV per NH_3 molecule by adding two or three more NH_3 molecules (Figure 5b and 5c), presumably the extra NH_3 molecules may disrupt the overall stability. Intriguingly, the highest binding energy of 0.25 eV per NH_3 molecule is obtained when six NH_3 molecules interconnected through H-bonding network with three linkers around the trigonal window (Figure 5d). Noticeably, the DFT optimised structures display the progressive distortion of the aligned bipyridine linkers with γ changed from 20.34 ° (which is well matched with the NPD refined desolvated structure of UiO-bpydc with no NH_3) to 19.47 °, 10.83 °, 9.49 °, and 6.33 ° by increasing the number of NH_3 molecules at the trigonal window (Figure 5a-d). Interestingly, for the case of UiO-bpydc with six NH_3 molecules (Figure 5d), the dihedral angles are twisted to nearly planar (γ = 6.33 °) in order to maximize the H-bonding geometry for all the molecules involved, which clearly corresponds to our NPD refined structure at 7 K at the highest loading (γ= 7.15(3)°), as shown in Table 2. According to our molecular modelling, the close inter-linked NH_3 molecules block up the trigonal window and prevent NH_3 molecules from entering the interior pore. These DFT results are in good agreement with the experimental observations and provide us with a further endorsement in the assembled H-bonding network with NH_3 adsorbates that governs the guest-responsive behaviors of this MOF-NH_3 system.

Table 2 | Summary of the dihedral angles between two aromatic rings of the linkers in UiO-67 and UiO-bpydc derived from Rietveld refinement of the NPD data. The number in round brackets are referred to as an estimated standard deviation.

Sample	Measurement Temperature (K)	Dihedral angle (degree) at the ND_3 loading of		
		0.00 mmol/g	4.63 mmol/g	7.60 mmol/g
UiO-67	300	30.06(1)	55.20(1)	62.63(2)
	7	27.94(1)	39.92(1)	ND[a]; 60.00(2)[b]
		0.00 mmol/g	4.27 mmol/g	6.06 mmol/g
UiO-bpydc	300	21.80(1)	16.77(3)	10.00(4)
	7	21.34(1)	16.04(2)	7.15(3)

[a]ND= Not determined at 7 K; [b] determined at 150 K

Table 3 | Summary of the dihedral angles between two aromatic rings of the linkers of UiO-bpydc obtained from DFT calculations at 0 K.

Sample	Dihedral angle (degree) with *n* NH_3 molecule(s) at the trigonal window[a]				
	n= 0	*n*= 1	*n*= 3	n= 4	n= 6
UiO-bpydc	20.33	19.47	10.83	9.49	6.33

[a] See the corresponding optimised structures in Figure 5

Structural Flexibility of Linker towards Stimuli

It is exciting to see from the DFT calculations that the flexibility of the linkers and pore structures can be subtly altered through the linker host-guest NH_3 interaction(s). As stated, the weak dipole-induced dipole interaction and strong H-bonding interaction as compared to thermal motions may give different structural variations. This can open up the new way of controlling molecular rigidity of linkers using NH_3 and temperature as stimuli. As a result, we also investigated how the temperature influences structural change, if any on the MOF-ND_3 systems, namely the UiO-67-ND_3 and UiO-bpydc-ND_3. Both their NPD patterns were measured at 300 K and/or 7 K and 150 K, respectively (Figure 6). Given the fact that the boiling and the melting points of ND_3 at 1 bar are 239.81 and 195.42 K, respectively, it is anticipated to see different degrees of rotation of the linkers induced by the adsorbed ND_3 over these temperatures.

To minimize the variance in ND_3 adsorption amount of each sample at different temperatures, the ND_3 gas uptake on the sample was first carried out and measured at room temperature, followed by isolation before cooling down to cryogenic temperature for further measurement. Thus, the NPD patterns were collected at 300 K for 20 minutes, and then at 7 K for 60 minutes (see SI). Due to constraints of allowed experimental time, NPD data of UiO-67 at the highest ND_3 dosing was collected at 150 K instead of the base temperature of 7 K in liquid helium but with satisfying data quality. No significant change in the patterns was observed for both ND_3-free MOFs (Figure 6a and 6e). Surprisingly, at the increasing ND_3 loading, dramatic changes of the peak intensities coupled with the formation of some small new Bragg peaks were found for the ND_3-loaded UiO-67 sample (Figure 6b-d and Figures S33- S35). The new peaks (marked with yellow asterisks in Figure 6i) were due to the orderly packing of the ND_3 molecules in the MOF framework.[33] Notice that the diffraction peaks primarily derived from the gas-free UiO-67 structure with flexible linkers were pronouncedly broadened and attenuated in the intensity at increasing ND_3 loading. Whilst the change in the structure factors due to the extra nuclear density of the ND_3 molecules can cause the broadening and the attenuation, we anticipate that the degree of ND_3 adsorption on the linker molecules (dipole-induced dipole interaction) and filling to inner porous sites may also likely create a range of structural distortions or/and disorder states to the linker, leading to a spread of population in closely related diffractions. The peaks attenuation appear to be more prominent at 7 K than 300 K (Figure 6l), which matches with the fact that the use of higher temperature with higher thermal energy can overcome the weak dipole-induced dipole interaction to set free the linkers from their distorted states. At high loading (L= 4.63), the additional peaks were clearly visible with the ordered ND_3 (Figure 6c). Interestingly, at the highest ND_3 loading, the use of high temperatures including 150 K and 300 K seems unable to overcome the interlocking forces from the cumulative dipole interactions, which retain the peaks broadening and attenuation. Clearly, the flexibility of the linkers is tunable by NH_3 loading and temperature applied to this system. Similar behaviors of the linker dynamics in rigid MOFs towards guest molecules and temperature were also observed by using a solid state ^2H NMR technique.[20, 46]

According to the refined models of UiO-67 shown in Figure 6j-l and of increasing ND_3 loading, the torsional distortion of the two biphenyl rings from 30.06 (1) ° is also varying due to the adsorbed ND_3 at different loading (for example, refined γ = 30.06 (1) ° at L= 0.00 can change to 55.20(1), and 63.62(2) ° at L= 4.63, and 7.60, respectively shown in Figure 6j and 6k and Table 2). This may be caused by the distortion to the hydrophobic linker with increasing amounts of hydrophilic guest molecules.[18-19, 46] Incredibly, these distinctive changes were totally prohibited in the presence of bipyridine linkers over the whole temperature regime in the case of UiO-bpydc (Figure 6f-h and Figures S37-S39). As seen from the Table 2, at increasing ND_3 loading, the dihedral angle of the two biphenyl rings this time becomes smaller (flattening) from 21.80(1)° at L= 0.00 to 16.77(3), and 10.00(4) ° at L= 4.27, and 6.60, respectively. Analysis of nuclear density residues was used to confirm the locations of the adsorbed ND_3 inside the MOF channels. For the ND_3-loaded UiO-67 samples, a dispersion of the nuclear density residues was observed when changing the measurement temperature from 7 K to 300 K (Figures S40 and S41). This finding was in sharp contrast to the UiO-bpydc at comparable ND_3 dosing where the pattern of the density residues clearly remained the same (Figures S42 and S43). According to the DFT calculations of the dihedral angles between two aromatic rings of the linker of UiO-bpydc, the strong H bonding indeed can flatten the dihedral angle and interlock with ammonia molecules accordingly to render rigidity of this linker over the wide temperature range with the same trend as observed in the experiments (Table 3).

It is known that the modification of the organic linkers with substituent groups and incorporation of guest molecules can change not only the electrostatic effect and equilibrium structure but also the rotational energy barrier (E_{rb}) of the organic linkers in the MOFs.[2] The E_{rb} values can indicate the flexibility of the linkers in MOF materials: the higher value of E_{rb}, the less flexibility of the MOF linkers. As a result, the E_{rb} values of the model MOFs were also calculated by DFT (see SI for details of these calculations), and the results are shown in Table S16. For the NH_3-free models, it is clearly found that the H_2bpydc linker of UiO-bpydc exhibits higher rotational barrier (0.55 eV) than the H_2bpdc of UiO-67 does (0.32 eV), revealing the less flexibility of the UiO-bpydc due to the substitution effects. More interestingly, the adsorption of NH_3 in the UiO-bpydc dramatically increases the E_{rb} to 0.64 eV, almost twice higher than that in the UiO-67 analogue. These computational results emphasize the strong influence of NH_3-MOF interactions on controlling the E_{rb} of the MOFs as well as their flexibility towards guest molecules which are in excellent agreement with the corresponding NPD experiments. These results support our initial hypothesis that the effect of thermal motion at elevated temperature may set free the rotation of the biphenyl scaffold ND_3 molecules inside the UiO-67 pores. In contrast, the ND_3-loaded UiO-bpydc could greatly suppress this linker flipping via a constraint of the stronger H-bonding network. An initial dynamics study by using an Inelastic Neutron Scattering (INS) technique also supports this responsive behavior of UiO-bpydc linker towards NH_3 inclusion (Figures S51 and S52). The decline of peak intensities associated to linker rotational modes of UiO-bpydc was much more prominent than those of UiO-67, implying a more restricted motion of the linker feasibly induced by H-bonding between NH_3 and bipyridine linkers. Further thermodynamic and kinetic studies and calculations are required in order to get a full understanding of the temperature-dependent and loading effects. This will highlight the importance of the molecular bonding interaction to lock up or set free molecular motion of linkers for controlling the responsive behavior of MOF materials with trapped guest molecules by external stimuli. At the uttermost exciting prospect, the ability to design and control the stimuli-responsive properties throughout linker motions might enable the development of artificial nanomachines for special usage.

CONCLUSION

High-resolution *in-situ* neutron diffraction along with Rietveld refinement and DFT calculations have been used to elucidate the structural responses of defective UiO-67 and its derivatives upon the inclusion of NH_3. It is demonstrated that the different pore openings (windows) induced by missing linkers can introduce stepped and hysteresis NH_3 sorption in UiO-type MOFs. Results also establish the influence of functional linkers of these isostructural MOFs on their NH_3 affinity and flexibility. The great alteration of stepped NH_3 adsorption behaviors can be taken place when the phenyl groups are replaced by the pyridine ones. This unusual adsorption transition results from the steric hindrance of H-bond networks between the bipyridine scaffold and the adsorbed NH_3 molecules, forcing the linkers to adopt planar geometry to block up the pore and made the structure temperature and NH_3 loading rigid. Moreover, the temperature-dependent neutron diffraction also reveals the NH_3-induced structural transformation of the organic linkers. We demonstrate, for the first time, that the structural flexibility of the linkers on UiO-type MOFs can play a significant role in the type of gas uptake dependent on temperature and guest loading without significant change in pore volume and unit cell parameters, which otherwise are believed to be rigid and non-interactive.

Understanding the structure-function relationship of the MOF-NH_3 systems will enable the rational design of potential materials with controllable properties for not only strongly interacting gas storage, but also other applications such as controlled drug delivery and molecular sensing upon the use of stimuli (temperature/guest molecules). Our study of utilising H-bonding interactions of NH_3 with tailored linkers (and healing) merited as the first example of this kind, which plays a key role to stabilise the dynamical structures of the flexible biphenyl group for stepwise adsorption of NH_3 without major structural or pore volume change. Ongoing efforts are focused on using neutron scattering and molecular dynamics simulations to establish the dynamic behaviors of this system with a controllable H-bond network.

EXPERIMENTAL SECTION

Full details of the experiments can be found in the SI.

Sample preparation. Defective UiO-67 was prepared according to a modified procedure based on the one reported by J. F. Cavka *et al.*[22] 8 mL of *N,N*-

dimethylformamide (DMF) was added into a glass vial containing 49 mg of zirconium tetrachloride ($ZrCl_4$), 378 mg of glacial acetic acid, and 52 mg of biphenyl-*4,4′*-dicarboxylic acid (H_2BPDC). The mixture was homogenized via sonication for 10 min, followed by solvothermal treatment at 393 K for 24 h. The solid product was washed with DMF three times, methanol three times, followed by methanol exchange for three days. During this period, methanol was exchanged daily. The final product was collected by centrifugation and activated at 423 K under vacuum for 12 h.

Defective UiO-bpydc[34] was prepared by using the procedure similar to that for UiO-67 synthesis, except 52 mg of *2,2′*-bipyridine-*5,5′*-dicarboxylic acid (H_2BPYDC) was used instead of H_2BPDC.

Laboratory characterization. X-ray powder diffraction (XRD) was performed by using a Bruker D8 Advance X-ray diffractometer operated at 40 kV and 40 mA with Cu Kα1 radiation (λ = 1.54056 Å). Thermogravimetric analysis (TGA) was performed on a TA Instruments TGA Q600 under an airflow of 100 ml/min. N_2 adsorption isotherm (at 77 K) up to 1 bar was analyzed using a micromeritics Tristar instrument. Before the sorption analysis, the sample (0.1−0.2 g) was loaded into a sample cell and subjected to a vacuum of 10^{-5} Torr at 423 K for 12 h. Temperature programmed ammonia desorption (NH_3-TPD) analysis was performed with a Micromeritics AutoChem II 2910 apparatus. The detection of desorbed molecules was done by a thermal conductivity detector. NH_3 sorption isotherms of the MOF samples were measured using a gas adsorption analyser (Quantachrome Autosorb iQ-Chemi). Each sample was placed in a chamber and outgassed under vacuum at 423 K for 24 h before measurement. 99.9 % NH_3 gas was loaded into the sample chamber at 298 K with a loading of 5 cm^3/time from 0 to 1000 mbar.

***In-situ* neutron powder diffraction (*In-situ* NPD).** *In-situ* NPD was conducted at WISH beamline[47], ISIS Neutron and Muon Source, Rutherford Appleton Laboratory, UK. The WISH instrument is a time-of-flight cold neutron diffractometer, primarily designed for powder diffraction at long *d*-spacing (0.7-50 Å) for magnetic and large unit cell systems. WISH is equipped with pixellated ^{3}He tube detectors covering almost the entire horizontal scattering plane (2θ range 10-170 ° on both sides). The scattering data are focused into five datasets at average 2θ values of 152.8, 121.6, 90.0, 58.3 and 27.1 ° of varying *d*-range and resolution. Prior to the measurement, the MOF sample was loaded into an 11 mm diameter vanadium can with quartz wool on top. The sample was degassed under high vacuum at 373 K for 24 h to remove any guest molecules. The sample holder was then transferred to a vacuum chamber connected to a custom-made gas loading system. An NPD pattern of the desolvated sample was first collected at 300 K for 20 min. After that, a He cryostat was used to cool down the sample can to 7 K, where the thermal motion of the MOF sample and adsorbed NH_3 molecules can be significantly reduced. High-resolution NPD of this sample was carried out at 7 K for 1 h to get good statistics. After the measurement, the sample was gently warmed up to 300 K before being dosed with NH_3 gas in a calibrated volume. Fully-deuterated ammonia (ND_3) was used owing to the large coherent neutron scattering of deuterium. Each of the loading steps required half an hour to enable the homogenous dispersion of ND_3 molecules inside the crystalline sample. The NPD patterns after each ND_3 loading were measured at 300 K and 7 K for 20 min and 1 h, respectively. For the low-temperature data collection at 7 K, the system was cooled down to 7 K slowly over 3 h in order to eliminate the gas condensation outside the sample.

Synchrotron powder X-ray diffraction (SXRD). SXRD data were collected on Beamline I11[48], Diamond Light Source, UK. The energy of the incident X-ray flux was set at 15 keV. The wavelength and the 2θ-zero point were refined using a diffraction pattern obtained from a high-quality silicon powder (SRM640c). High-resolution SXRD data of all samples were achieved by using the multi-analyser crystals (MAC) detectors in the 2θ range 0-150 ° with 0.001 ° data binning. Each MAC pattern was collected for an hour to get satisfying statistics.

Density Functional Theory (DFT) calculations. Spin-polarized DFT calculations were carried out using the Perdew-Burke-Ernzerhof (PBE)[39] exchange–correlation functional by using the Vienna *ab initio* Simulation Package (VASP).[40] Details of the DFT calculations can be found in the SI.

ASSOCIATED CONTENT

Supporting Information. Experimental details, supplementary characterization results, and additional data analysis. This material is available free of charge via the Internet at http://pubs.acs.org.

CCDC 2047200, 2047201, 2047202, 2047203, 2047204, and 2047205 contain the supplementary crystallographic data for this paper. The data can be obtained free of charge from The Cambridge Crystallographic Data Centre via www.ccdc.cam.ac.uk/structures.

AUTHOR INFORMATION

Corresponding Author

*Email: edman.tsang@chem.ox.ac.uk (S. C. E. Tsang); xpwu@ecust.edu.cn (X.-P. Wu)

Author contributions

#These authors contributed equally.

ACKNOWLEDGEMENTS

ISIS Neutron and Muon Source (UK) is gratefully thanked for providing the NPD and INS facilities. The SXRD facilities provided by both Diamond Light Source (UK) and Spring 8 (Japan) are also acknowledged. T.Y. thanks The Development and Promotion for Science and Technology Talents project (DPST, Thailand) for financial support. P.Z. thanks the University of Oxford for a Glasstone research fellowship. X.-P.W. thanks Shanghai Sailing Program (20YF1410000) for funding.

Competing financial interests

The authors declare no competing financial interests.

Additional information

The data that support the findings of this study are available from the corresponding authors on request.

REFERENCES

1. Budrikis, Z., Making the Switch. *Nat. Rev. Mater.* **2018,** *3* (6), 72-72.
2. Gonzalez-Nelson, A.; Coudert, F.-X.; van der Veen, M. A., Rotational Dynamics of Linkers in Metal–Organic Frameworks. *Nanomaterials* **2019,** *9* (3), 330-366.
3. Krause, S.; Hosono, N.; Kitagawa, S., Chemistry of Soft Porous Crystals: Structural Dynamics and Gas Adsorption Properties. *Angew. Chem. Int. Ed.* **2020,** *59* (36), 15325-15341.
4. Zhou, H.-C.; Long, J. R.; Yaghi, O. M., Introduction to Metal–Organic Frameworks. *Chem. Rev.* **2012,** *112* (2), 673-674.
5. Kitagawa, S.; Kitaura, R.; Noro, S.-i., Functional Porous Coordination Polymers. *Angew. Chem. Int. Ed.* **2004,** *43* (18), 2334-2375.
6. Easun, T. L.; Moreau, F.; Yan, Y.; Yang, S.; Schröder, M., Structural and Dynamic Studies of Substrate Binding in Porous Metal–Organic Frameworks. *Chem. Soc. Rev.* **2017,** *46* (1), 239-274.
7. Karmakar, A.; Samanta, P.; Desai, A. V.; Ghosh, S. K., Guest-Responsive Metal–Organic Frameworks as Scaffolds for Separation and Sensing Applications. *Acc. Chem. Res.* **2017,** *50* (10), 2457-2469.
8. Wu, X.-P.; Gagliardi, L.; Truhlar, D. G., Cerium Metal–Organic Framework for Photocatalysis *J. Am. Chem. Soc.* **2018,** *140* (25), 7904-7912.
9. Zhao, P.; Fang, H.; Mukhopadhyay, S.; Li, A.; Rudić, S.; McPherson, I. J.; Tang, C. C.; Fairen-Jimenez, D.; Tsang, S. C. E.; Redfern, S. A. T., Structural Dynamics of a Metal–Organic Framework Induced by CO_2 Migration in Its Non-Uniform Porous Structure. *Nat. Commun.* **2019,** *10* (1), 999.
10. Krause, S.; Bon, V.; Senkovska, I.; Stoeck, U.; Wallacher, D.; Többens, D. M.; Zander, S.; Pillai, R. S.; Maurin, G.; Coudert, F.-X.; Kaskel, S., A Pressure-Amplifying Framework Material with Negative Gas Adsorption Transitions. *Nature* **2016,** *532*, 348.
11. Yang, S.; Lin, X.; Lewis, W.; Suyetin, M.; Bichoutskaia, E.; Parker, J. E.; Tang, C. C.; Allan, D. R.; Rizkallah, P. J.; Hubberstey, P.; Champness, N. R.; Mark Thomas, K.; Blake, A. J.; Schröder, M., A Partially Interpenetrated Metal–Organic Framework for Selective Hysteretic Sorption of Carbon Dioxide. *Nat. Mater.* **2012,** *11* (8), 710-716.
12. Zhang, S.-Y.; Jensen, S.; Tan, K.; Wojtas, L.; Roveto, M.; Cure, J.; Thonhauser, T.; Chabal, Y. J.; Zaworotko, M. J., Modulation of Water Vapor Sorption by a Fourth-Generation Metal–Organic Material with a Rigid Framework and Self-Switching Pores. *J. Am. Chem. Soc.* **2018,** *140* (39), 12545-12552.
13. McDonald, T. M.; Mason, J. A.; Kong, X.; Bloch, E. D.; Gygi, D.; Dani, A.; Crocellà, V.; Giordanino, F.; Odoh, S. O.; Drisdell, W. S.; Vlaisavljevich, B.; Dzubak, A. L.; Poloni, R.; Schnell, S. K.; Planas, N.; Lee, K.; Pascal, T.; Wan, L. F.; Prendergast, D.; Neaton, J. B.; Smit, B.; Kortright, J. B.; Gagliardi, L.; Bordiga, S.; Reimer, J. A.; Long, J. R., Cooperative Insertion of CO_2 in Diamine-Appended Metal-Organic Frameworks. *Nature* **2015,** *519* (7543), 303-308.
14. Gu, C.; Hosono, N.; Zheng, J.-J.; Sato, Y.; Kusaka, S.; Sakaki, S.; Kitagawa, S., Design and Control of Gas Diffusion Process in a Nanoporous Soft Crystal. *Science* **2019,** *363* (6425), 387.
15. Cho, H. S.; Yang, J.; Gong, X.; Zhang, Y.-B.; Momma, K.; Weckhuysen, B. M.; Deng, H.; Kang, J. K.; Yaghi, O. M.; Terasaki, O., Isotherms of Individual Pores by Gas Adsorption Crystallography. *Nat. Chem.* **2019,** *11* (6), 562-570.
16. Fairen-Jimenez, D.; Moggach, S. A.; Wharmby, M. T.; Wright, P. A.; Parsons, S.; Düren, T., Opening the Gate: Framework Flexibility in ZIF-8 Explored by Experiments and Simulations. *J. Am. Chem. Soc.* **2011,** *133* (23), 8900-8902.
17. Krause, S.; Bon, V.; Stoeck, U.; Senkovska, I.; Többens, D. M.; Wallacher, D.; Kaskel, S., A Stimuli-Responsive Zirconium Metal–Organic Framework Based on Supermolecular Design. *Angew. Chem. Int. Ed.* **2017,** *56* (36), 10676-10680.
18. Kanoo, P.; Matsuda, R.; Sato, H.; Li, L.; Hosono, N.; Kitagawa, S., Pseudo-Gated Adsorption with Negligible Volume Change Evoked by Halogen-Bond Interaction in the Nanospace of MOFs. *Chem. Eur. J.* **2020,** *26* (10), 2148-2153.
19. Bärwinkel, K.; Herling, M. M.; Rieß, M.; Sato, H.; Li, L.; Avadhut, Y. S.; Kemnitzer, T. W.; Kalo, H.; Senker, J.; Matsuda, R.; Kitagawa, S.; Breu, J., Constant Volume Gate-Opening by Freezing Rotational Dynamics in Microporous Organically Pillared Layered Silicates. *J. Am. Chem. Soc.* **2017,** *139* (2), 904-909.
20. Jiang, X.; Duan, H.-B.; Khan, S. I.; Garcia-Garibay, M. A., Diffusion-Controlled Rotation of Triptycene in a Metal–Organic Framework (MOF) Sheds Light on the Viscosity of MOF-Confined Solvent. *ACS Cent. Sci.* **2016,** *2* (9), 608-613.
21. Krause, S.; Evans, J. D.; Bon, V.; Senkovska, I.; Iacomi, P.; Kolbe, F.; Ehrling, S.; Troschke, E.; Getzschmann, J.; Többens, D. M.; Franz, A.; Wallacher, D.; Yot, P. G.; Maurin, G.; Brunner, E.; Llewellyn, P. L.; Coudert, F.-X.; Kaskel, S., Towards General Network Architecture Design Criteria for Negative Gas Adsorption Transitions in Ultraporous Frameworks. *Nat. Commun.* **2019,** *10* (1), 3632.
22. Cavka, J. H.; Jakobsen, S.; Olsbye, U.; Guillou, N.; Lamberti, C.; Bordiga, S.; Lillerud, K. P., A New Zirconium Inorganic Building Brick Forming Metal Organic Frameworks with Exceptional Stability. *J. Am. Chem. Soc.* **2008,** *130* (42), 13850-13851.
23. Shearer, G. C.; Chavan, S.; Bordiga, S.; Svelle, S.; Olsbye, U.; Lillerud, K. P., Defect Engineering: Tuning the Porosity and Composition of the Metal–Organic Framework UiO-66 via Modulated Synthesis. *Chem. Mater.* **2016,** *28* (11), 3749-3761.
24. Cliffe, M. J.; Wan, W.; Zou, X.; Chater, P. A.; Kleppe, A. K.; Tucker, M. G.; Wilhelm, H.; Funnell, N. P.; Coudert, F.-X.; Goodwin, A. L., Correlated Defect Nanoregions in a Metal–Organic Framework. *Nat. Commun.* **2014,** *5* (1), 4176.
25. Wu, H.; Chua, Y. S.; Krungleviciute, V.; Tyagi, M.; Chen, P.; Yildirim, T.; Zhou, W., Unusual and Highly Tunable Missing-Linker Defects in Zirconium Metal–Organic Framework UiO-66 and Their Important Effects on Gas Adsorption. *J. Am. Chem. Soc.* **2013,** *135* (28), 10525-10532.
26. Forgan, R. S.; Marshall, R. J.; Struckmann, M.; Bleine, A. B.; Long, D.-L.; Bernini, M. C.; Fairen-Jimenez, D., Structure-Directing Factors when Introducing Hydrogen Bond Functionality to Metal–Organic Frameworks. *CrystEngComm* **2015,** *17* (2), 299-306.
27. Yang, Q.-Y.; Lama, P.; Sen, S.; Lusi, M.; Chen, K.-J.; Gao, W.-Y.; Shivanna, M.; Pham, T.; Hosono, N.; Kusaka, S.; Perry Iv, J. J.; Ma, S.; Space, B.; Barbour, L. J.; Kitagawa, S.; Zaworotko, M. J., Reversible Switching between Highly Porous and Nonporous Phases of an Interpenetrated Diamondoid Coordination Network That Exhibits Gate-Opening at Methane Storage Pressures. *Angew. Chem. Int. Ed.* **2018,** *57* (20), 5684-5689.
28. Lama, P.; Barbour, L. J., Distinctive Three-Step Hysteretic Sorption of Ethane with In Situ Crystallographic Visualization of the Pore Forms in a Soft Porous Crystal. *J. Am. Chem. Soc.* **2018,** *140* (6), 2145-2150.
29. Sikiti, P.; Bezuidenhout, C. X.; van Heerden, D. P.; Barbour, L. J., Direct in Situ Crystallographic Visualization of a Dual Mechanism for the Uptake of CO_2 Gas by a Flexible Metal–Organic Framework. *Inorg. Chem.* **2019,** *58* (13), 8257-8262.
30. Rieth, A. J.; Dincă, M., Controlled Gas Uptake in Metal–Organic Frameworks with Record Ammonia Sorption. *J. Am. Chem. Soc.* **2018,** *140* (9), 3461-3466.
31. Rieth, A. J.; Hunter, K. M.; Dincă, M.; Paesani, F., Hydrogen Bonding Structure of Confined Water Templated by a Metal-Organic Framework with Open Metal Sites. *Nat. Commun.* **2019,** *10* (1), 4771.
32. Leroux, M.; Mercier, N.; Allain, M.; Dul, M.-C.; Dittmer, J.; Kassiba, A. H.; Bellat, J.-P.; Weber, G.; Bezverkhyy, I., Porous Coordination Polymer Based on Bipyridinium Carboxylate Linkers with High and Reversible Ammonia Uptake. *Inorg. Chem.* **2016,** *55* (17), 8587-8594.
33. Barter, M.; Hartley, J.; Yazigi, F.-J.; Marshall, R. J.; Forgan, R. S.; Porch, A.; Jones, M. O., Simultaneous Neutron Powder Diffraction and Microwave Dielectric Studies of Ammonia

Absorption in Metal–Organic Framework Systems. *Phys. Chem. Chem. Phys.* **2018,** *20* (15), 10460-10469.

34. Gonzalez, M. I.; Bloch, E. D.; Mason, J. A.; Teat, S. J.; Long, J. R., Single-Crystal-to-Single-Crystal Metalation of a Metal–Organic Framework: A Route toward Structurally Well-Defined Catalysts. *Inorg. Chem.* **2015,** *54* (6), 2995-3005.

35. Li, L.; Tang, S.; Wang, C.; Lv, X.; Jiang, M.; Wu, H.; Zhao, X., High Gas Storage Capacities and Stepwise Adsorption in a UiO Type Metal–Organic Framework Incorporating Lewis Basic Bipyridyl Sites. *Chem. Commun.* **2014,** *50* (18), 2304-2307.

36. Gutov, O. V.; Hevia, M. G.; Escudero-Adán, E. C.; Shafir, A., Metal–Organic Framework (MOF) Defects under Control: Insights into the Missing Linker Sites and Their Implication in the Reactivity of Zirconium-Based Frameworks. *Inorg. Chem.* **2015,** *54* (17), 8396-8400.

37. Sears, V. F., Neutron Scattering Lengths and Cross Sections. *Neutron News* **1992,** *3* (3), 26-37.

38. Young, R. A., *The Rietveld Method*. International Union of Crystallograhy: Chester, England, 1993.

39. Coelho, A., TOPAS and TOPAS-Academic: an Optimization Program Integrating Computer Algebra and Crystallographic Objects Written in C++. ++. *J. Appl. Crystallogr.* **2018,** *51* (1), 210-218.

40. Ko, N.; Hong, J.; Sung, S.; Cordova, K. E.; Park, H. J.; Yang, J. K.; Kim, J., A Significant Enhancement of Water Vapour Uptake at Low Pressure by Amine-Functionalization of UiO-67. *Dalton Trans.* **2015,** *44* (5), 2047-2051.

41. Trickett, C. A.; Gagnon, K. J.; Lee, S.; Gándara, F.; Bürgi, H.-B.; Yaghi, O. M., Definitive Molecular Level Characterization of Defects in UiO-66 Crystals. *Angew. Chem. Int. Ed.* **2015,** *54* (38), 11162-11167.

42. Øien-Ødegaard, S.; Shearer, G. C.; Wragg, D. S.; Lillerud, K. P., Pitfalls in Metal–Organic Framework Crystallography: towards More Accurate Crystal Structures. *Chem. Soc. Rev.* **2017**, *46* (16), 4867-4876.

43. Godfrey, H. G. W.; da Silva, I.; Briggs, L.; Carter, J. H.; Morris, C. G.; Savage, M.; Easun, T. L.; Manuel, P.; Murray, C. A.; Tang, C. C.; Frogley, M. D.; Cinque, G.; Yang, S.; Schröder, M., Ammonia Storage by Reversible Host–Guest Site Exchange in a Robust Metal–Organic Framework. *Angew. Chem. Int. Ed.* **2018,** *57* (45), 14778-14781.

44. Hewat, A. W.; Riekel, C., The Crystal Structure of Deuteroammonia between 2 and 180 K by Neutron Powder Profile Refinement. *Acta Cryst. A* **1979,** *35* (4), 569-571.

45. Matthias, T.; Katsumi, K.; Alexander, V. N.; James, P. O.; Francisco, R.-R.; Jean, R.; Kenneth, S. W. S., Physisorption of Gases, with Special Reference to the Evaluation of Surface Area and Pore Size Distribution (IUPAC Technical Report). *Pure Appl. Chem.* **2015,** *87* (9-10), 1051-1069.

46. Inukai, M.; Tamura, M.; Horike, S.; Higuchi, M.; Kitagawa, S.; Nakamura, K., Storage of CO_2 into Porous Coordination Polymer Controlled by Molecular Rotor Dynamics. *Angew. Chem. Int. Ed.* **2018,** *57* (28), 8687-8690.

47. Chapon, L. C.; Manuel, P.; Radaelli, P. G.; Benson, C.; Perrott, L.; Ansell, S.; Rhodes, N. J.; Raspino, D.; Duxbury, D.; Spill, E.; Norris, J., Wish: The New Powder and Single Crystal Magnetic Diffractometer on the Second Target Station. *Neutron News* **2011,** *22* (2), 22-25.

48. Thompson, S. P.; Parker, J. E.; Potter, J.; Hill, T. P.; Birt, A.; Cobb, T. M.; Yuan, F.; Tang, C. C., Beamline I11 at Diamond: A new instrument for high resolution powder diffraction. *Rev. Sci. Instrum.* **2009,** *80* (7), 075107.

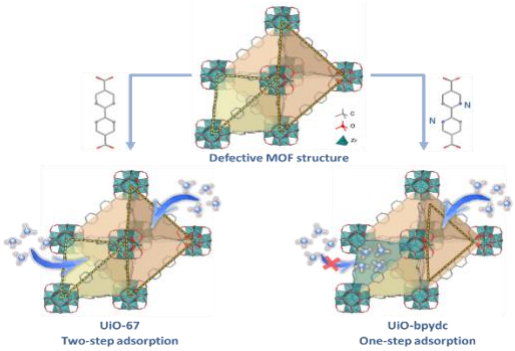

Table of Contents Only